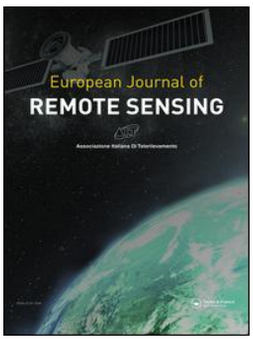

European Journal of Remote Sensing

ISSN: (Print) 2279-7254 (Online) Journal homepage: http://www.tandfonline.com/loi/tejr20

Ground deformation and associated hazards in NW peloponnese (Greece)

Matteo Del Soldato, Chiara Del Ventisette, Federico Raspini, Gaia Righini, Valeria Pancioli & Sandro Moretti

To cite this article: Matteo Del Soldato, Chiara Del Ventisette, Federico Raspini, Gaia Righini, Valeria Pancioli & Sandro Moretti (2018) Ground deformation and associated hazards in NW peloponnese (Greece), European Journal of Remote Sensing, 51:1, 710-722, DOI: 10.1080/22797254.2018.1479622

To link to this article: https://doi.org/10.1080/22797254.2018.1479622

Published online: 09 Jul 2018.

EUROPEAN JOURNAL OF REMOTE SENSING
2018, VOL. 51, NO. 1, 710–722
https://doi.org/10.1080/22797254.2018.1479622

Ground deformation and associated hazards in NW peloponnese (Greece)

Matteo Del Soldato [a], Chiara Del Ventisette [a], Federico Raspini[a], Gaia Righini[b], Valeria Pancioli[c] and Sandro Moretti [a]

[a]Department of Earth Sciences, University of Firenze, Florence, Italy; [b]ENEA, Italian National Agency for New Technologies, Energy and Sustainable Economic Development, Bologna, Italy; [c]Agenzia per la Sicurezza Territoriale e la Protezione Civile Regione Emilia-Romagna, Bologna, Italy

ABSTRACT

In the last decades, ground deformations were investigated, analysed and monitored using several methods. As a consequence of a spreading urbanization, several phenomena, e.g. landslide and subsidence, were emphasized or triggered causing not only socio-economic damages, but, in some cases, also casualties. The investigation and mapping of these phenomena are important for both local authorities and civil protection in order to promote a higher conscientious urban planning and to highlight the more hazardous areas. Furthermore, the information are a key point for social development connected to the awareness of the environment and the related risk. The Achaia prefecture, in the north-eastern Peloponnese (Greece), close to the Gulf of Patras, is an area strongly affected by subsidence and landslides. Furthermore, this is an earthquake-prone area, a factor that can trigger some mass movements. For this region, a landslide inventory was realized with the help of the interpretation of Persistent Scatterers data, for the period 1992–2008, and high-resolution optical satellite images, available until 2016, in addition to the investigation of the landslide State of Activity. Moreover, for the coastal area, a section was investigated to evidence subsidence.

ARTICLE HISTORY
Received 15 November 2017
Revised 14 May 2018
Accepted 18 May 2018

KEYWORDS
Landslide; subsidence; Greece; PSInSAR; state of activity

Introduction

In the last two decades, the continuous urbanization due to the population growth increased the risk related to the ground deformation hazard in areas landslide-, subsidence- and earthquake prone as the north-western part of Peloponnese, Greece.

Frequently, moderate-to-large earthquakes afflict the Gulf of Corinth (e.g. Briole et al., 2000; Hatzfeld et al., 2000; Bernard et al., 2006) and the Gulf of Patras (e.g. Beckers et al., 2015; Gobo, Ghinassi, Nemec, Sjursen, & Hampson, 2014) triggering off numerous mass movements and causing subsidences.

Subsidence and landslide phenomena affecting urbanized areas generate important social and economic losses (Klose, Damm, & Terhorst, 2015; Schuster & Highland, 2001;) in addition to important damage on structures and infrastructures (Bianchini, Nolesini, Del Soldato, & Casagli, 2017; Ciampalini et al., 2014; Del Soldato et al., 2017, 2016). To reduce the cost of disasters influencing regions affected by multi-risks, a proper land management and planning play a key role (Del Ventisette, Righini, Moretti, & Casagli, 2014; Guzzetti et al., 2012). The development of multi-interferogram approaches (Ferretti et al., 2011; Ferretti, Prati, & Rocca, 2001) have helped to make a step ahead in landslide research and monitoring applications since the early 2000s (Bozzano et al., 2017; Colesanti & Wasowski, 2006; Del Ventisette et al., 2013; Solari et al., 2018). Moreover, the free availability of high-resolution optical images and the possibility to combine all information on GIS platforms, have given many benefits in terms of costs, time and field work (Farina, Colombo, Fumagalli, Marks, & Moretti, 2006). Indeed, the combination of remote sensing techniques, in this case A-DInSAR study and image-interpretation, allowed the investigation of wide areas in the northwest of Peloponnese, Greece.

The aim of this work is to improve the knowledge on landslide and subsidence phenomena affecting the territory and to investigate the reliability of the simultaneous use of ancillary and remote sensing data to estimate ground deformations in order to evaluate the correlated hazards in the Achaia prefecture. Territory featured by urbanized and rural areas affected by deformations due to landslides and subsidence phenomena.

The combination of different types of data allowed to have a better overview and to cover wide areas, including both urbanized and vegetated regions. Photo and radar interpretation are the starting points to create a landslide inventory (Govi, 1977; Nichol & Wong, 2005; Van Westen, 2000). The

CONTACT Matteo Del Soldato matteo.delsoldato@unifi.it Department of Earth Sciences, University of Firenze, Florence, Italy

image-interpretation is an essential tool to detect landslides in wide areas also covered by vegetation (Brardinoni, Slaymaker, & Hassan, 2003), while the radar-interpretation allows better results in the urbanized area (Farina, Casagli, & Ferretti, 2007; Ferretti et al., 2001).

In this work, a landslides inventory with the evaluation of the State of Activity (SoA) was developed by means of simultaneous image- and radar-interpretations. The creation of a reliable landslide inventory can support a better land and emergency managing of territory affected by urban expansion. Furthermore, the subsidence involving the coastal part of the Achaia prefecture (northern Peloponnese, Greece) was analysed by means of Persistent Scatterers Interferometry and the subsidence rate in some sample areas was evaluated. Detection, measurement and monitoring of subsidence, mainly close to urbanized areas, were important to evaluate the effects caused by the expansion of the urban centres.

Study area

The study area is located in the northwest coastal region of the Peloponnese, separated by the Gulf of Corinth from the Greek mainland. This region is identified as one of the most rapidly developed intercontinental rifts in the Mediterranean area. The area of interest, located between Patrasso and Ziria, Achaia prefecture, is an area partially but heavily urbanized that extends to about 200 km^2 (Figure 1(a)).

Geological setting

The evolution of the Gulf of Corinth involved the formations of the northern part of the Peloponnese accommodating the associated extension due to theactive subduction between the African and European plates (Koukis et al., 2009).

The geology of the area was investigated assembling several maps of the *Institute of Geology & Mineral Exploration – IGME-GR* (Greek Geological Survey). The faulting is widespread in all the northern part of the Peloponnese area and faults resulted active during Plio-Pleistocene with consequences in the sedimentary column of the Quaternary formations. The lithology of the Peloponnese was grouped in six main units, from the bottom to the top (Figure 1(b)):

- *Zarouchla unit* composed by quartzites, quartz-phyllites and pelitic schists; thin irregular alternations limestone beds and sericite schists; metavolcanic rocks; various metaclastic lithologies; green and violet sandy schists; intercalations of small calcarenitic lenses (Katagas, Tsolis-Katagas, & Baltatzis, 1991);
- *Gavrovo-Tripolis* unit composed by carbonate sedimentary rocks of shallow marine environment, sometimes dolomitized (Cretaceous-Upper Triassic) and Eocene-Upper Oligocene flysch derived from Mesozoic platform (Nikas, Antonakos, Lambrakis, & Kallergis, 2007). Formations with more than 1000 m of thickness of limestone, dolomite and dolomitic limestone;
- *Olonos-Pindos* unit is characterized by calcareous sedimentary rocks and pelagic sediments derived from the Mesozoic ocean basin

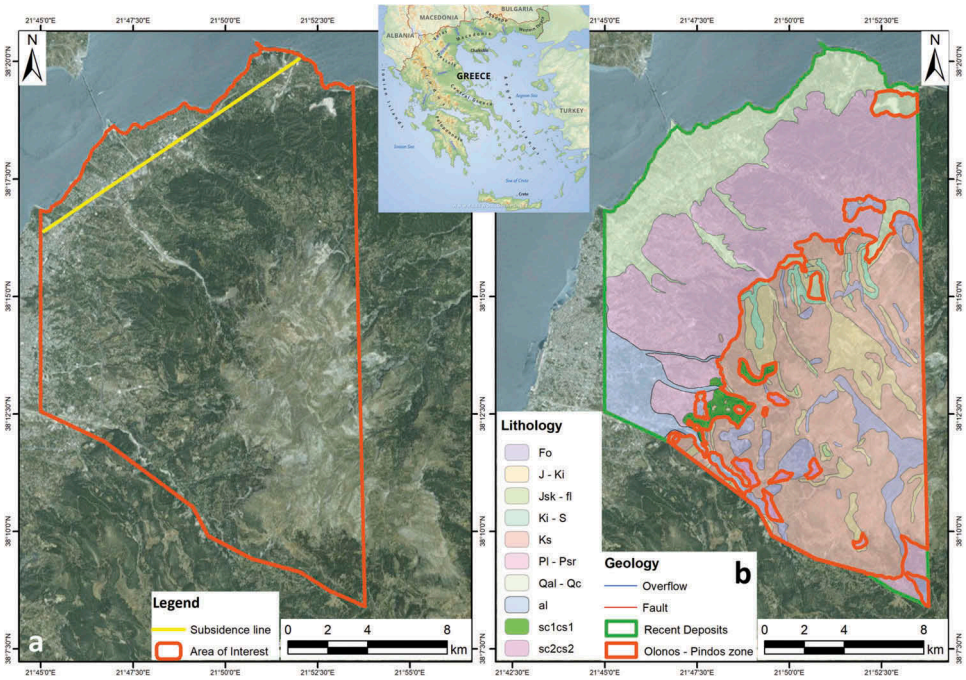

Figure 1. Localization of the area of interest (a) and detailed lithology (b) of the Achaia region, NW Peloponnesus, Greece.

accumulated on the passive margin (Piper, 2006): sandy, silty and more rarely conglomerate flysch (Fo), sporadic Upper Cretaceous – Eocene pelagic limestone (Ks), pelagic limestones with thin intercalations and siliceous nodules, cherts and limestones (Ki – S) with intercalations of argillaceous shale and marls (Lower – Upper Cretaceous). Jurassic – Lower Cretaceous reddish, white and microcrystalline siliceous layers with sporadic levels of calcareous algae and red radiolarites (J – Ki). Some tectonic window of Upper Triassic formation (Jsk – fl) composed by platy limestone and flysch of clay, sandstone and marls.

- *Recent deposits* mantling the coastal region, is alternation of transgressive and regressive sedimentation of lacustrine and marine-lacustrine material subsequently evolved in several deltas as Gilbert-type, and influencing the production of relevant thickness of Plio-Pleistocene sediments (Koukis et al., 2009; Ori, 1989). Torrential weathering (al) and alluvium deposits (Qal – Qc), in which recent (Holocene) and older (Pleistocene), more consolidated, talus cones (sa1cs1 – sc2cs2) are in evidence in the coastal region. Fine-grained materials result from both vertically and horizontally phases of development composing these geomorphological shapes. At the back, there are the marine brackish and lacustrine deposits of the Plio-Pleistocene period (Pl – Psr).
- *Sedimentary-tectonic complex and detachment rocks* are respectively the olistolite formation blocks from the overhead series and different elements associated to the above. The dimensions of the block are more variable and derived from different allochthonous formations.
- *Schists and Volcanic rocks* are present in a small extent and form the basement of the sedimentary Alpine series often through tectonic contacts.

The last two classes, tectonics and volcanic rocks, were maintained separated from the others due to their different geotechnical characteristics.

Available data and methodology

The study area was investigated using a Digital Elevation Model (DEM) with 20 m cell resolution, derived maps and ancillary data, in addition to high-resolution optical images and PSI (Persistent Scatterer Interferometry) products. Relevant parameters for the conducted analysis were the slope, and the lithology of the area (derived by merging and digitalizing *IGME* maps).

The main support to the investigation was provided by means of C-band radar data from ERS1/2 and ENVISAT satellites, available for the area of interest from 1992 to 2008 (Table 1). All the images were captured with a Line Of Sight (LOS) of 23° with respect to the vertical and a vertical polarization (VV). In addition to the SAR images, optical data on Google Earth Pro covering for the whole investigated area until 2015 were taken into account. Over the area, several images were available until to 2015: the first images covering the entire scenario date back 2003 but only from about 2010 they have a good temporal resolution to make a precise interpretation. A regular time span is impossible to have due to the cloudy covering. These resources permitted to analyse the SoA of many landslides as well as to identify and evaluate the spatial distribution of landslide phenomena. The radar images were processed by Telerilevamento Europa s.r.l. through the PSInSAR technique (Ferretti, Prati, & Rocca, 2000; Ferretti et al., 2001) generating Persistent Scatterers (PS) outputs.

Table 1. Time period and number of permanent scatterers (PS) of satellite data sets in the investigated area.

Satellite	Track	Images number	Time Period	n° PS	Orbit angle (°)	Ground resolution (m)
ERS desc	T279	39	19,922,000	17,250	≈ 101	25
ERS desc	T7	35	19,922,000		≈ 101	25
ENVISAT asc	T145	19	20,022,008	1639	≈ 259	30
ENVISAT desc	T279	25	20,022,008	6601	≈ 101	30

A pre-processing analysis showed that the possible geometrical distortion, relevant to have a more awareness in the investigation and interpretation of the products (Novellino et al., 2017), is low influence and the following track were chosen in order to capture as many as possible slope.

The sample region shows an average distribution of PS data of about 127.7 PS km^{-2}, concentrated in the coastal area due to a spreading urbanization (Figure 2).

The different density of PS between ERS and ENVISAT satellite is due to the different number of the used images in the processing as well as in the different spatial resolution, i.e. 25 m and 30 m, respectively, for ERS and ENVISAT, in as much the incident and inclinationangle are the same for both satellites. The ground deformations at regional scale were mapped through the integration of the SAR interferometry products with high-resolution optical satellite images and thematic maps (e.g. Del Soldato et al., 2016; Del Ventisette et al., 2013; Farina et al., 2006; Tofani, Del Ventisette, Moretti, & Casagli, 2014). Taking into account these characteristics, the merging of data by superimposing the PS data on the high-resolution images (Bianchini et al., 2012; Farina et al., 2006) was fundamental for an exhaustive interpretation. In Figure 3 the flow chart of the work is illustrated.

The high-quality optical images analysis permits to recognize the morphological shapes and features associated with large and medium mass movements that also in vegetated areas can be recognized, while

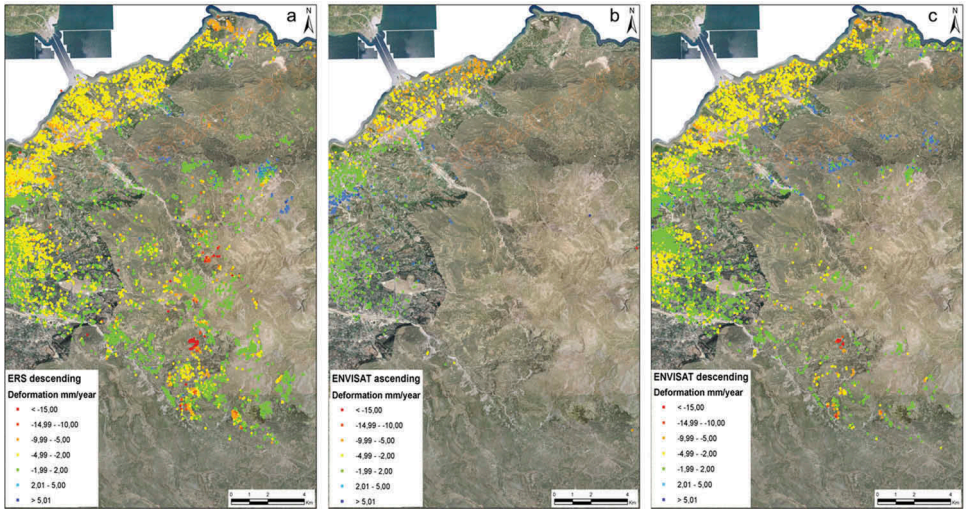

Figure 2. PS products by ERS descending (a), ENVISAT ascending (b) and descending (c) in the Achaia prefecture, NW of Peloponnese.

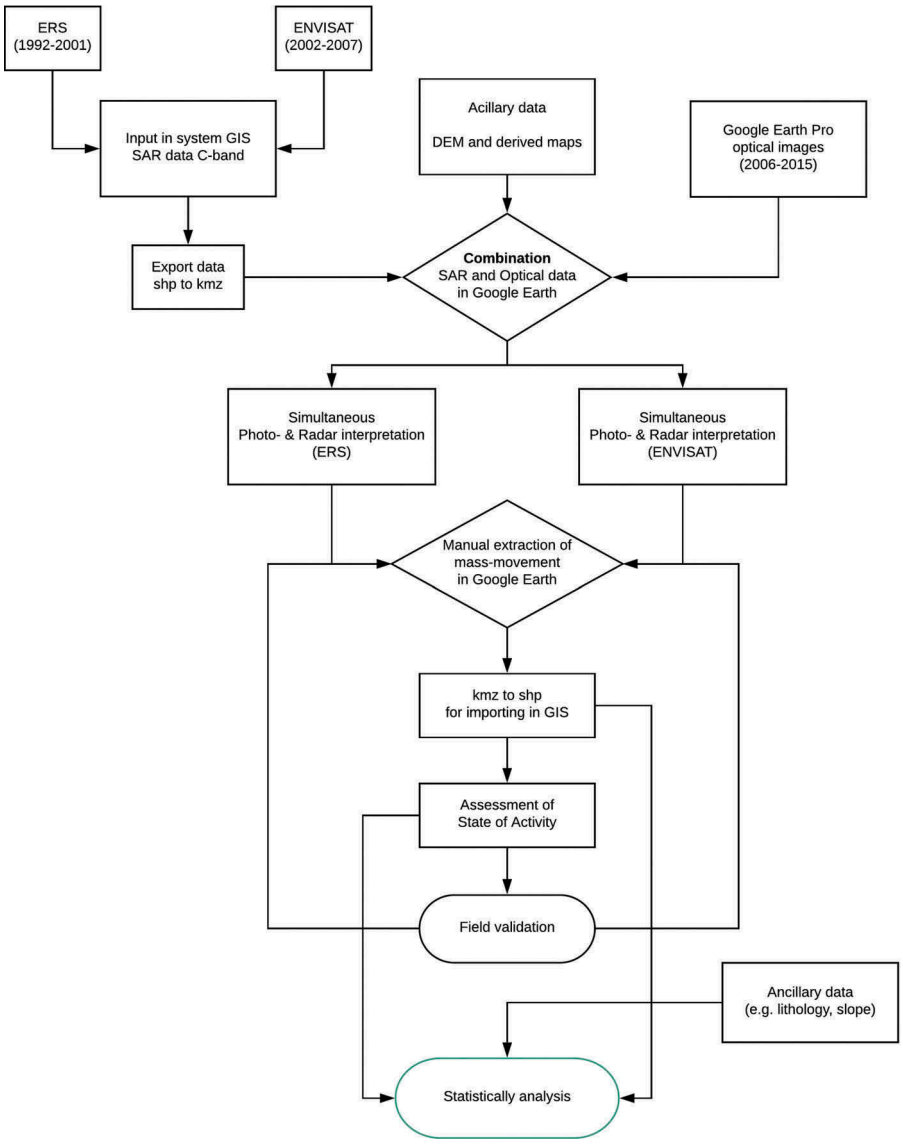

Figure 3. Flow chart of the work.

for the small failures, field surveys are in any case necessary. To interpret the optical images, the area was hypothetically divided in sub-section and they were manually controlled to look for denudated areas or anomalous changes of vegetation. Once identified an area with these characteristics, all the

available images of other dates were analysed, and the presence and derivable information of PS were checked. The procedure to combine the results of the two methodologies is commonly used to map ground deformations such as landslides (Bianchini et al., 2012; Casagli, Colombo, Ferretti, Guerri, & Righini, 2008; Farina et al., 2007; Righini, Pancioli, & Casagli, 2012) and subsidence (Galloway & Burbey, 2011; Raspini, Loupasakis, Rozos, Adam, & Moretti, 2014; Raspini, Loupasakis, Rozos, & Moretti, 2013) as well as to investigate the spatial distribution and kinematic evidence related to ground deformation risks.

The scattering due to the spread vegetation, the threshold based on the wavelength of the instrument, as well as the exposition of the target with respect to the satellite LOS, the chance to observe only slow displacements are the main restriction in the identification and monitoring of landslides. In any case, information about spatial distribution, temporal evolution, type of movement and geometry of landslides can be extracted. A standard palette is used to visualize the PS using colours that characterize the values of the displacement: hot colours for negative values, indicating an increase of the distance between the target and the sensor; cold colours for positive values, revealing reduction of the gap; green for the stability range of ±2 mm/y. The stability range was established according to the standard deviation deriving on the processing chain.

This approach allowed the study of the SoA back in time. A long time series of images was investigated to retrieve the SoA of the mass movements permitting to recognize morphological and displacement evolution (e.g. Cigna, Bianchini, & Casagli, 2013; Strozzi, Ambrosi, & Raetzo, 2013). The multi-temporal photo-interpretation (Guzzetti, Carrara, Cardinali, & Reichenbach, 1999) and the radar-interpretation support the discrimination of the SoA thanks to reflecting elements, such as nude outcrops, roads, buildings, that allow to recognize displacements or movements affecting them. The analysis of the SoA was carried out combining the higher mean velocities between ascending and descending PS on mass movements recognized in the investigated areas by ERS1/2 (1992–2001) and ENVISAT (2002–2007) data applying the activity matrix identifying nine different classes of activity (Table 2). A further back analysis to investigate a longer time-evolution was impossible to realize because a previous landslide inventory was not available.

In case of absence of PS on landslide, in ERS or ENVISAT datasets, the SoA was assessed using categories considering the two possibilities that can be occurred with the presence of the missing data (Righini et al., 2012). In these cases, the image-interpretation of pictures shot in the same period or successively with respect to ENVISAT can help to investigate the evolution of the phenomena, even if no values of velocity of movement can be estimated with this method.

The SoA made by means of the velocity of displacement by PS is tied until 2007. For further evolutions and for phenomena where no PS are present, the high-resolution optical images were used to investigate their development in time.

Furthermore, the PSI approach resulted useful to investigate subsidence widespread in the north-western coastal area (Figure 4). A section in the coastal area involved by subsidence was traced and the PS contained in a buffer of 50 m were examined in order to analyse the subsidence ground effects. The PS were interpolated by means of the *Inverse Distance Weighted* (IDW) method (Shepard, 1968), based on the weighted average of the neighbourhood PS following the role that more the distance between the known point increase, more the weight of its values decrease.

The sensor-target displacement, the projection of the real motion along the LOS, can be estimated through the PS interferometry. To obtain the real vertical deformation (Vv), the measured displacement (ΔLOS) has to be corrected by the look angle (θ°) of the LOS:

$$Vv = \frac{\Delta LOS}{\cos \theta}$$

Table 2. Landslide State of Activity matrix from ERS and ENVISAT.

		ERS		
		No V ≤ 2 mm/year	V > 2 mm/year	No data
ENVISAT	V ≤ 2 mm/year	*Stabilized*	*Reactivated*	*Stabilized* / *Reactivated*
	V > 2 mm/year	*Dormant*	*Active Continuous*	*Dormant* / *Active Continuous*
	No data	*Dormant* / *Stabilized*	*Active* / *Continuous Reactivated*	*No info photointerpretation*

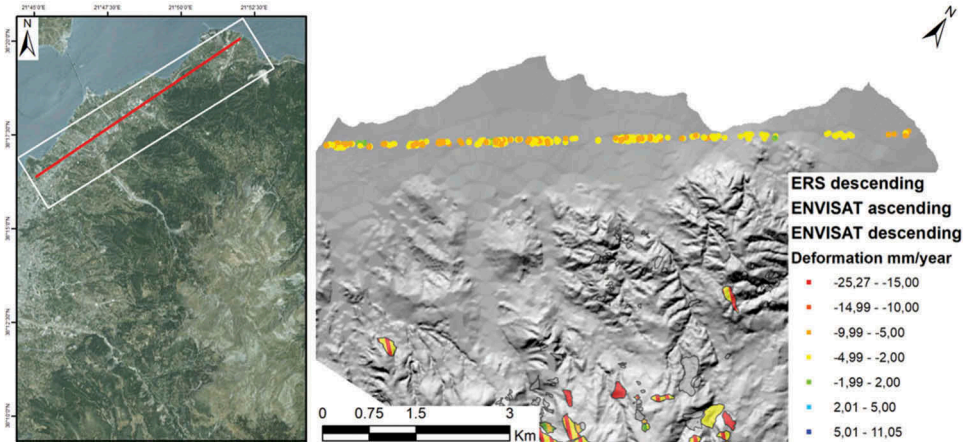

Figure 4. PS products along the traced section to investigate the subsidence of the coastal area of the Achaia prefecture, NW of Peloponnese.

By means of the interpolation of average velocity acquired by PS for the buffer zone, a subsidence profile can be generated to investigate the displacement that affected the coastal region.

Data analysis and results

Combining image- and radar interpretation, more than 600 mass movements were recognized and traced (Figure 5(a)). This approach permits to investigate the whole territory affected by mass movements. Furthermore, for about 300 landslides, the SoA analysis (Figure 5(b)) was detected (Table 3).

The major number of the categorized landslides falls into the *Dormant/Active continuous* class or *Active continuous* category.

Examples of two landslides areas are here individually reported.

The first area is located southern with respect to the municipality of Mintzeika, Achaia, where a group of landslides were mapped and classified as *Active continuous* (Righini et al., 2012) due to the presence of both ERS and ENVISAT descending data with annual mean velocity values up to 10 mm/year (Figure 6).

During the field trip carried out in June 2009, the reliability of the radar-interpretation was checked for most of the movements. In particular for the Achaia south-west part, many unstable areas were identified mainly along the road network where cracks or scarps in the road fill showed landslides evidence; indeed, a consistent correspondence between PS and significant damage on the main road was evident and

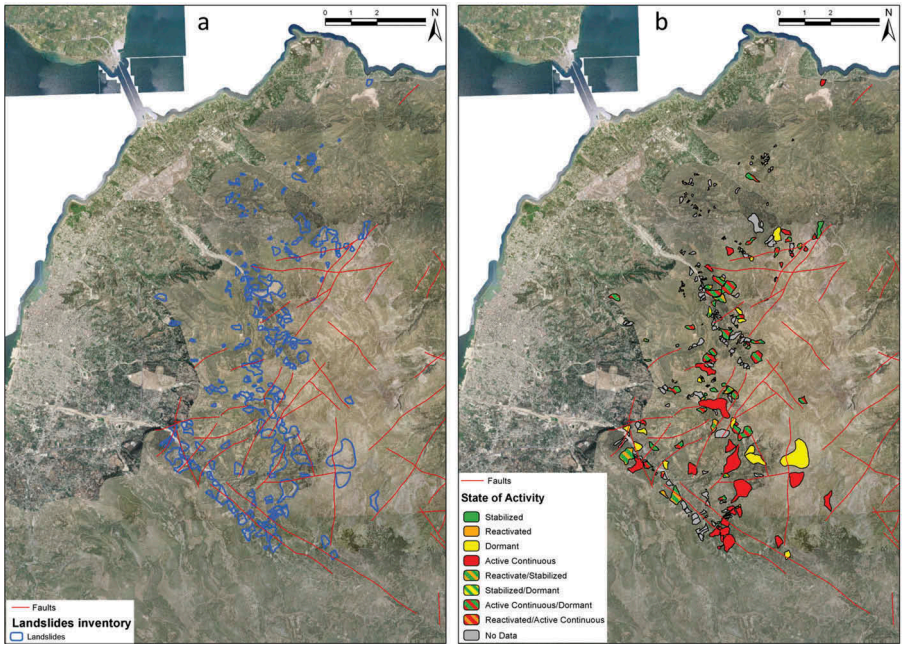

Figure 5. Landslides inventory (a) classified based on the SoA detected by the ERS1/2 and ENVISAT PS data from 1992 to 2008 (b).

Table 3. Summary of classification of the state of activity of the landslides.

Stabilized	3
Reactivated	1
Dormant	14
Active continuous	27
Reactivated/Stabilized	16
Stabilized/Dormant	2
Active continuous/Dormant	45
Reactivated/Active continuous	3
No categorized	194

many displacements were also evident on some cement barriers and nets (Figure 7(a,d)). Moreover, a panoramic overview of deformations behaviour was observed on several slopes (Figure 7(b)) characterised by horizontal displacements, especially near the landslide foot, stronger vertical components very near to the crown of the landslide and scarcity of growing vegetation such as bushes or grass, on the main landslide body (Figure7(c)).

The second area concerns a mass movement located in the centre of the investigated area of the NW of the Peloponnese (red circle in Figure 8(a)). Close to Choradro village, three important landslides affecting the same basin were recognized and analysed (Figure 8(a)). Only ERS data (Figure 8(b)) were collected, no ENVISAT data were recorded, and

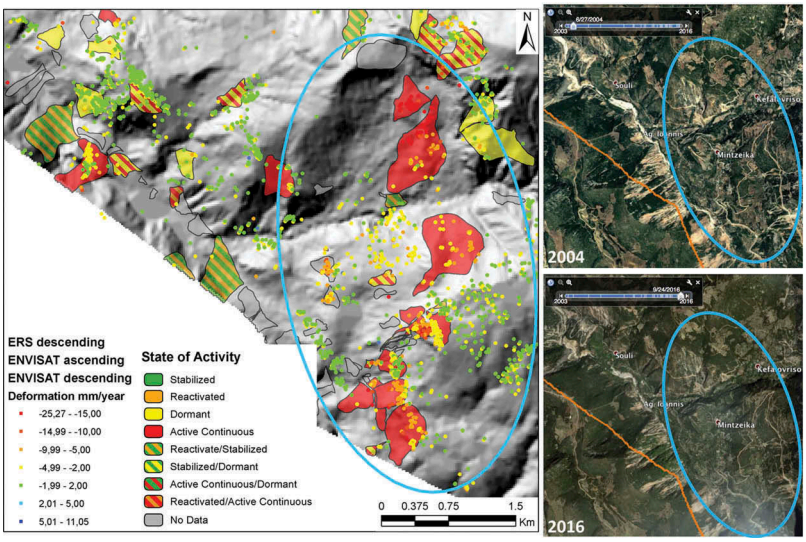

Figure 6. Landslides area (blue circle) affected by active mass movement in Achaia south-west part.

Figure 7. Picture captured during the field surveys conducted on selected landslides to validate the results obtained by remote sensing interpretations.

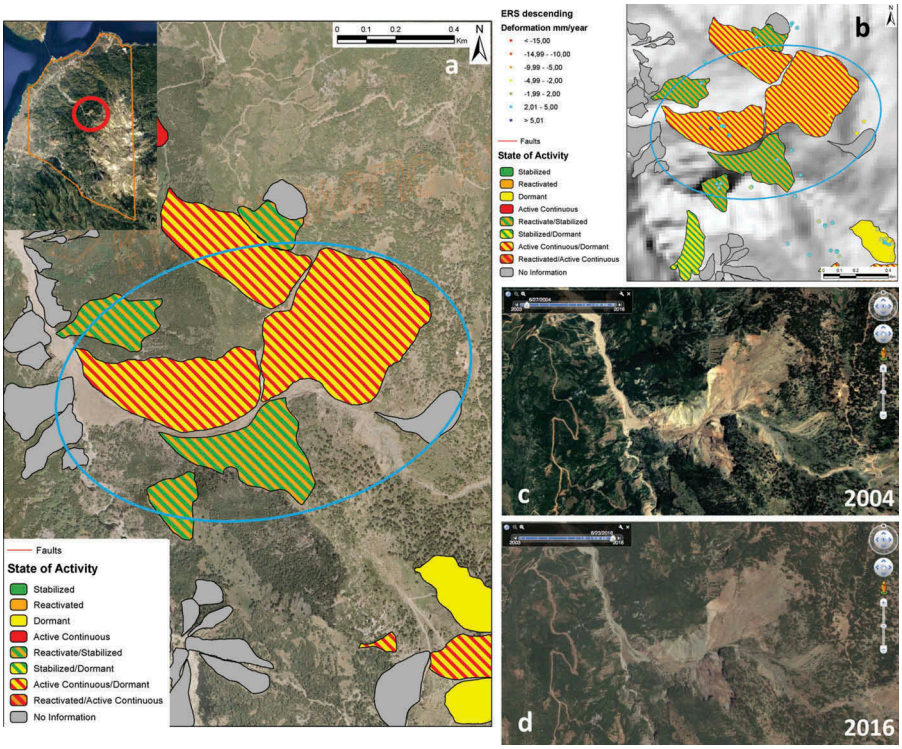

Figure 8. (a) Second sample area affected by three landslides investigated (in light-blue circle). (b) ERS descending data on the area of interest. High-resolution satellite images shot on 2004 (c) and 2016 (d), respectively.

high-resolution images of different years are available to control the possible evolution of the landslide. According to (Righini et al., 2012) the classification based on the SoA, two landslides in this area are categorized as *Dormant/Active continuous* and one as *Stabilized/Dormant*. The high-resolution images from 2004 (Figure 8(c)) to 2016 (Figure 8(d)) suggest that, as in the last decades, all the investigated landslides seem not to show any increment of dimensions. Without ENVISAT PS data and only with optical images, the velocity of displacement is undeterminable and it is not possible to discriminate the SoA. Taking advantage of the availability of the optical images, it is possible to suppose that the landslide could be *Dormant* or *Stabilized*, because no increment of dimension or new denudated areas are recognizable.

Moreover, the analysis of the PS velocities in the flat urbanized coastal region of the area of interest, built over Quaternary formations, shows negative deformation rates. This area results interested by subsidence close to the main urban centre, showing deformation rates reaching values up to 10 mm/year. Several villages/locations exhibit subsidence rates of particular interest, e.g. Agios Vesileios, a village in the municipality of Rio, showing velocities exceeding 7.5 mm/year. To investigate the subsidence affecting the coastal area, a section was traced through the urbanized centres from Valtos municipality, in the western coast, to Arachovitika, a village in the municipal unit of Rio (Fig. 9(a)). The section line, about 12 km long, intersects the sedimentary cones and urbanized areas where PSs suggest relevant negative displacements. The same limit of stability of ±2 mm/year was used to analyse and identify the subsidence hazard.

The PS data of ERS (Fig. 9(b)) and ENVISAT (Fig. 9(c)), were analysed, identifying three areas characterized by significant subsidence recognizable in both profiles, highlighted with red, yellow and blue stripes.

The area highlighted in yellow in (Fig. 9) is superimposed on sedimentary alluvial deposits cones and close to an industrialized area. These could justify the important value of subsidence identified by means of the PS analysis along the section with a maximum value of −6.3 mm/year. The area coloured in red is close to the mouth of a river almost completely filled by alluvial deposits. Furthermore, in the area where the section was traced several industrial constructions are present. It allows to suppose that the subsidence is caused the combination of compaction of the sedimentations and over-pumping of water. In this area, the highest value of subsidence was recorded by the ERS1/2 data reaching about −8.95 mm/years. The blue area is close to Arachovitika where a river is partially filled by alluvial sediments. Moreover, this area is featured by a low density urbanization mostly devoted to cultivation and agricultural fields. This can suggest that the subsidence could be related to high rate of water pumping. Also in this area, the highest rate recorded during the ERS1/2 period reached a maximum value of about −6.6 mm/year.

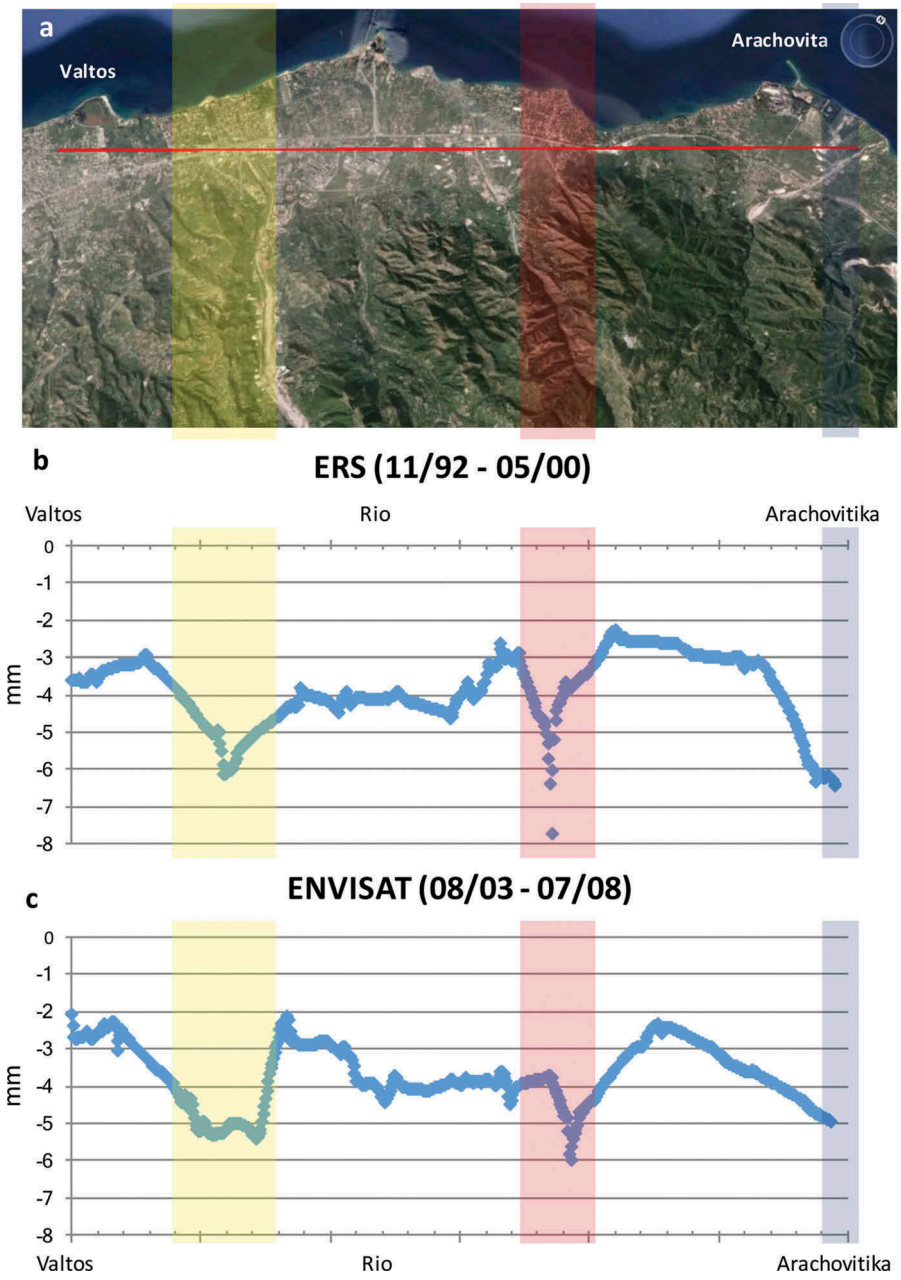

Figure 9. Section line (red line in a) traced to analyse the ERS (b) and ENVISAT (c) subsidence profile along the section. The areas with important subsidence are highlighted in yellow, red and blue. For a precise localization of the section see Figure 4.

Time series of a representative ERS and ENVISAT point inside the three zones highly affected by the subsidence (Figure 10) show two phases: (i) in the ERS period (1993–2000) there are low displacements, but cyclical; (ii) the ENVISAT period is featured by a more constant displacement, mainly in the yellow and red areas, with less influence due to cyclical trend.

Discussion and conclusions

The main purpose of this work was to improve background knowledge offering a synoptic view of the deformations caused by extensive natural disaster phenomena, such as landslides and subsidence, affecting the NW region of Peloponnese, Greece, through the simultaneous radar- and image interpretation. Furthermore, a field observation for several landslides was carried out to have validation of the resulting interpretation. The potentialities of the image-interpretation and the SAR interferometry are largely exploited in literature on both landslide and subsidence phenomena. ERS and ENVISAT data combined with high-resolution optical images were analysed in order to realize a landslide inventory with an assessment of the SoA. In this case, a previously existing landslide inventory of the region of interest was not available. It would be an important information to correlate the interpreted PS data with the ground truth (Psychogyiou et al., 2015). The results of this work confirmed the potential of multi-interferometric InSAR data to support landslide investigation at

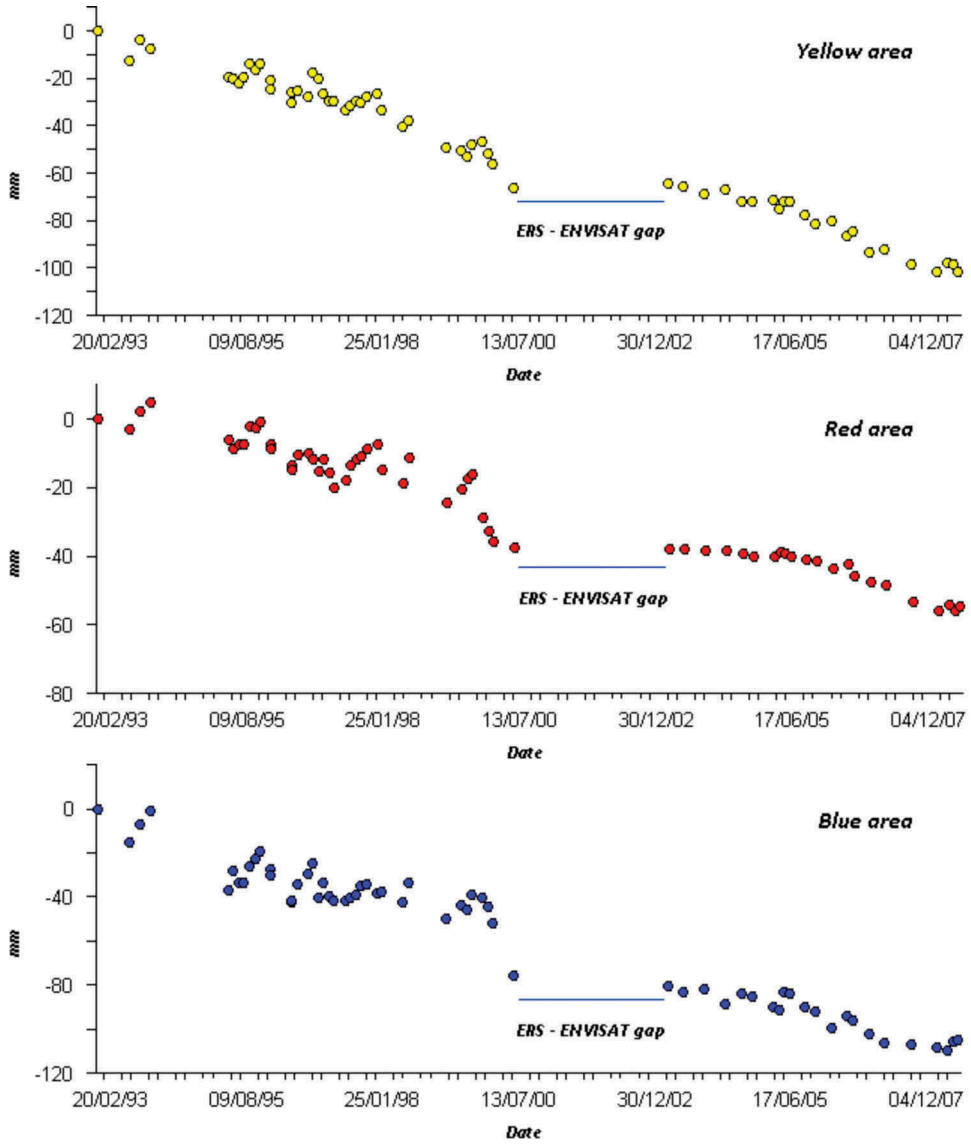

Figure 10. Sample of the time series measured along the LOS by PS ERS and ENVISAT in the three sample PS in the areas affected by subsidence and coloured as in the previous image in yellow, red and blue.

regional scale and the contribution for sustainable urban planning and infrastructure development. The main limitations of the PSI techniques, such as not enough benchmarks or the low availability and reliability on vegetated area, were overcome by means of the use of high-resolution satellite images. In this way, it was possible to investigate wide urbanized and vegetated areas for a long period, from 1993 to 2016.

More than 600 landslides were recognized mainly concentrated in the hinterland of the region of interest; the major number of them were categorized as *Active continuous/Dormant* and *Active Continuous*, but several mass movements are featured by absence of PS data (Figure 11,4). This confirms the relevant contribution of the high-resolution images for the spread vegetation in the area. It is worth noticing that using optical images the velocity of displacement is impossible to assess, but the image-interpretation results to be, in any case, a fundamental support to investigate the evolution of the mass movements by identifying the growing of the vegetation or the extension of sliding and nude areas.

Statistical analyses between the number of the landslides recognized, SoA, involved lithology and slope gradient were conducted. Combining the number of the landslides with the lithology it is possible to recognize a predominance of involvement of the "Ks" formation, belonging to the Olonos-Pindos zone, a pelagic limestone strictly connected with the sandy, silty and more rarely conglomerate flysch (Fo) (Figure 11(a)). In the study of the South Pindus mountain range, one of the main affected formation was the flysch of Pindos zones (Psychogyiou et al., 2015) as occurred in this case of study. Analysing the relationship between the slope and the distribution of the landslide (Figure 11(b)), it is possible to observe that between 15–25 and 25–35 degrees quite all the mass movements occurred (42% and 36%, respectively). The third investigation shows the relationship between the SoA and the number of landslides. In this case, the analysis was conducted only

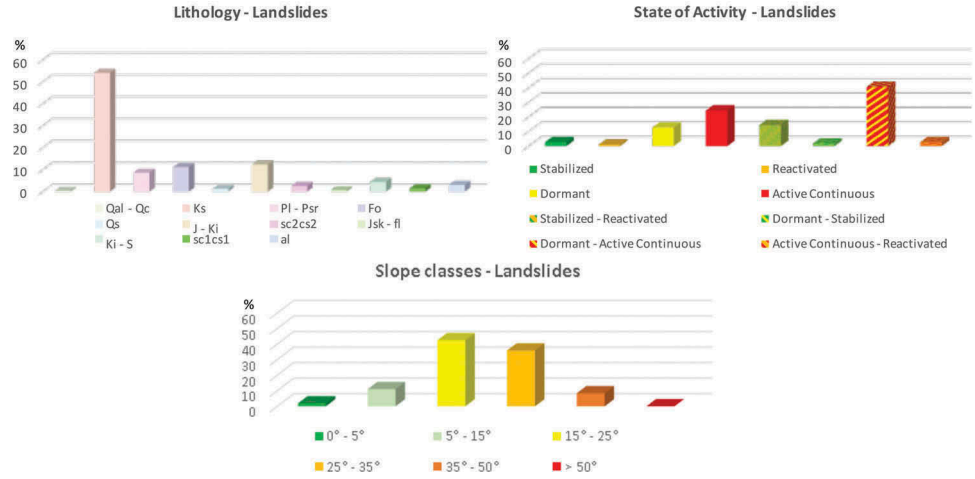

Figure 11. Statistical analysis of the landslide with respect to the lithology (a), the SoA (b) and the slope classes (c).

on the 300 landslides for which the SoA were assessed. The *Active Continuous* and *Active Continuous/Dormant* in addition to a less percentage of *Dormant* and *Dormant/Stabilized* classes represent the entire set of landslides (Figure 11(c)). Furthermore, in Table 4, the distinction for each class of SoA was related with every lithology unit.

The result of the work is a landslide inventory map supplied by the SoA and a subsidence section in the coastal area useful for land management and urban planning, in addition to civil protection purposes. The combination of different remote sensing approaches and ancillary data, as demonstrated in literature (e.g. Del Ventisette et al., 2014) and in this work, represents a valuable tool and a sustainable method, in terms of time and costs, to investigate landslide inventory and SoA of urbanized and vegetated wide areas.

Taking advantage of the spread of PS data in the coastal area subsidence rates were investigated and detected by means of an analysis along a section, principally close to the mouth of the rivers and the urbanized centres. The analysis of the time series of the PS and their location with respect to the lithology and geomorphology allow to suppose that the subsidence is caused by the combination of the possible compaction of alluvial sediments and the over-pumping of the water. It is important to report that bigger displacements and cyclical trends were recorded by the ERS data with respect to the ENVISAT.

The time series of the three areas affected by subsidence were shown by means of a representative point of each zone both in ERS and ENVISAT. For each area, they show a trend of moving away from the sensor in addition to a cyclical one, trends usually identified in cases of over-pumping mainly remarked for the ERS period. It results comparable with the hypothesis of contribution of over-pumping and compaction of sedimentary soils. The cyclical trend is less recognizable in the ENVISAT data, probably because the over-pumping was controlled and reduced.

At the end the obtained maps are important tools for civil protection purposes, for urban managing and planning as well as useful information for the society. The results can help the population to be awareness to the exposition to risk.

A consistent improvement of this work could come from recent satellite constellations, e.g. Sentinel-1, in order to monitor the evolution of the landslide displacement, to categorize the presently SoA and to investigate the evolution of the subsidence in the coastal areas. Furthermore, with more data and with high spatial resolution, landslide and subsidence effects on structures and infrastructures could be investigated (Herrera et al., 2010; Ciampalini et al., 2014; Sanabria et al., 2014; Bianchini et al., 2017; Del Soldato et al., 2017; 2018).

Table 4. Distribution of each class of the state of activity of the landslide related to every present lithology.

SoA vs Lithology	al	Fo	J – Ki	Jsk -fl	Ki – S	Ks	Pl – Psr	Qal – Qc	sc1cs1	sc2cs2
Stabilized	0	1	2	0	0	3	0	1	0	3
Reactivated	0	0	0	0	0	1	0	0	0	0
Dormant	0	4	9	2	1	18	2	0	2	1
Active Continuous	1	10	9	0	0	**38**	3	4	2	2
Reactivated/Stabilized	2	6	11	4	5	13	2	1	1	2
Stabilized/Dormant	0	0	1	0	0	3	0	0	0	0
Active Continuous/ Dormant	2	9	7	0	10	**52**	4	1	1	0
Reactivated/Active Continuous	0	0	0	0	0	4	0	0	1	0
No data	8	31	41	1	31	181	65	1	5	9

Acknowledgements

This research was funded by the European Space Agency (ESA) within the framework of the Terrafirma project. Special thanks to Nikos Nikolaou and Natalia Spanou of the Institute of Geology and Mineral Exploration (IGME) of Greece for their support in the collection of ancillary data and help during the field trip.

Disclosure statement

No potential conflict of interest was reported by the authors.

Funding

This research was funded by the European Space Agency (ESA) within the framework of the Terrafirma project.

ORCID

Matteo Del Soldato http://orcid.org/0000-0001-7539-5850
Chiara Del Ventisette http://orcid.org/0000-0003-2429-7710
Sandro Moretti http://orcid.org/0000-0002-1167-2721

References

Bernard, P., Lyon-Caen, H., Briole, P., Deschamps, A., Boudin, F., Makropoulos, K., Papadimitriou, P., Lemeille, F., Patau, G., Billiris, H., Paradissis, D., Papazissi, K., Castarède, H., Charade, O, Nercessian, A., Avallone, A., Pacchiani, F., Zahradnik, J., Sacks, S., Linde, A. (2006). deformation and seismic hazard in the western rift of Corinth: New insights from the Corinth Rift Laboratory (CRL). *Tectonophysics*, *426*(1–2), 7–30.

Beckers, A., Hubert-Ferrari, A., Beck, C., Bodeux, S., Tripsanas, E., Sakellariou, D., & De Batist, M. (2015). Active faulting at the western tip of the Gulf of Corinth, Greece, from high-resolution seismic data. *Marine Geology*, *360*, 55–69.

Bianchini, S., Cigna, F., Righini, G., Proietti, C., & Casagli, N. (2012). Landslide hotspot mapping by means of persistent scatterer interferometry. *Environmental Earth Sciences*, *67*(4), 1155–1172.

Bianchini, S., Nolesini, T., Del Soldato, M., & Casagli, N. (2017). *Evaluation of Building Damages Induced by Landslides in Volterra Area (Italy) Through Remote Sensing Techniques*. Workshop on World Landslide Forum (pp. 111–120). Springer, Cham.

Bozzano, F., Mazzanti, P., Perissin, D., Rocca, A., De Pari, P., & Discenza, M.E. (2017). Basin Scale Assessment of Landslides Geomorphological Setting by Advanced InSAR Analysis. *Remote Sensing*, *9*(3), 267.

Brardinoni, F., Slaymaker, O., & Hassan, M.A. (2003). Landslide inventory in a rugged forested watershed: A comparison between air-photo and field survey data. *Geomorphology*, *54*(3–4), 179–196.

Briole, P., Rigo, A., Lyon-Caen, H., Ruegg, J.C., Papazissi, K., Mitsakaki, C., … Deschamps, A. (2000). Active deformation of the Corinth rift, Greece: Results from repeated Global Positioning System surveys between 1990 and 1995. *Journal of Geophysical Research: Solid Earth*, *105*(B11), 25605–25625.

Casagli, N., Colombo, D., Ferretti, A., Guerri, L., & Righini, G. (2008). *Case study on local landslide risk management during crisis by means of remote sensing data*. Proceedings of the First World Landslide Forum, Tokyo Japan.

Ciampalini, A., Bardi, F., Bianchini, S., Frodella, W., Del Ventisette, C., Moretti, S., & Casagli, N. (2014). Analysis of building deformation in landslide area using multisensor PSInSAR™ technique. *International Journal of Applied Earth Observation and Geoinformation*, *33*, 166–180. Retrieved from http://www.sciencedirect.com/science/article/pii/S0303243414001317

Cigna, F., Bianchini, S., & Casagli, N. (2013). How to assess landslide activity and intensity with Persistent Scatterer Interferometry (PSI): The PSI-based matrix approach. *Landslides*, *10*(3), 267–283.

Colesanti, C., & Wasowski, J. (2006). Investigating landslides with space-borne Synthetic Aperture Radar (SAR) interferometry. *Engineering Geology*, *88*(3–4), 173–199.

Del Soldato, M., Bianchini, S., Calcaterra, D., De Vita, P., Martire, D.D., Tomás, R., & Casagli, N. (2017). A new approach for landslide-induced damage assessment.Geomatics. *Natural Hazards and Risk*, 8(2), 1524–1537.

Del Soldato, M., Di Martire, D., Bianchini, S., Tomás, R., De Vita, P., Ramondini, M., … Calcaterra,, D. (2018). An assessment of landslide-induced damage to structures: Agnone (southern Italy) case study. *Bulletin of Engineering Geology and the Environment*. doi:10.1007/s10064-018-1303-9

Del Soldato, M., Roberto Tomás, R., Pont, J., Herrera, G., Uan Carlos García Lopez-Davalillos, U.C.G.L.-D., & Mora, O. (2016). A multi-sensor approach for monitoring a road bridge in the Valencia harbor (SE Spain) by SAR Interferometry (InSAR). *Rendiconti Online Della Società Geologica Italiana*, *41*, 235–238.

Del Ventisette, C., Ciampalini, A., Manunta, M., Calò, F., Paglia, L., Ardizzone, F., … Guzzetti, F. (2013). Exploitation of large archives of ERS and ENVISAT C-band SAR data to characterize ground deformations. *Remote Sensing*, *5*(8), 3896–3917.

Del Ventisette, C., Righini, G., Moretti, S., & Casagli, N. (2014). Multitemporal landslides inventory map updating using spaceborne SAR analysis. *International Journal of Applied Earth Observation and Geoinformation*, *30*, 238–246.

Farina, P., Casagli, N., & Ferretti, A. (2007). *Radar-interpretation of InSAR measurements for landslide investigations in civil protection practices*. First North American Landslide Conference.

Farina, P., Colombo, D., Fumagalli, A., Marks, F., & Moretti, S. (2006). Permanent Scatterers for landslide investigations: Outcomes from the ESA-SLAM project. *Engineering Geology*, *88*(3–4), 200–217.

Ferretti, A., Fumagalli, A., Novali, F., Prati, C., Rocca, F., & Rucci, A. (2011). A new algorithm for processing interferometric data-stacks: SqueeSAR. *IEEE Transactions on Geoscience and Remote Sensing*, *49*(9), 3460–3470.

Ferretti, A., Prati, C., & Rocca, F. (2000). Nonlinear subsidence rate estimation using permanent scatterers in differential SAR interferometry. *IEEE Transactions on Geoscience and Remote Sensing*, *38*(5), 2202–2212.

Ferretti, A., Prati, C., & Rocca, F. (2001). Permanent scatterers in SAR interferometry. *IEEE Transactions on Geoscience and Remote Sensing*, *39*(1), 8–20.

Galloway, D.L., & Burbey, T.J. (2011). Revisão: Subsidência regional associada à extracção de água subterrânea. *Hydrogeology Journal*, *19*(8), 1459–1486.

Gobo, K., Ghinassi, M., Nemec, W., Sjursen, E., & Hampson, G. (2014). Development of an incised valley-fill at an evolving rift margin: Pleistocene eustasy and tectonics on the southern side of the Gulf of Corinth, Greece. *Sedimentology*, *61*(4), 1086–1119.

Govi, M. (1977). Photo-interpretation and mapping of the landslides triggered by the Friuli earthquake (1976). *Bulletin of Engineering Geology and the Environment*, *15*(1), 67–72.

Guzzetti, F., Carrara, A., Cardinali, M., & Reichenbach, P. (1999). Landslide hazard evaluation: A review of current techniques and their application in a multi-scale study, Central Italy. *Geomorphology*, *31*(1–4), 181–216.

Guzzetti, F., Mondini, A.C., Cardinali, M., Fiorucci, F., Santangelo, M., & Chang, K.-T. (2012). Landslide inventory maps: New tools for an old problem. *Earth-Science Reviews*, *112*(1–2), 42–66.

Hatzfeld, D., Karakostas, V., Ziazia, M., Kassaras, I., Papadimitriou, E., Makropoulos, K., … Papaioannou, C. (2000). Microseismicity and faulting geometry in the Gulf of Corinth (Greece). *Geophysical Journal International*, *141*(2), 438–456.

Herrera, G., Tomás, R., Monells, D., Centolanza, G., Mallorquí, J.J., Vicente, F., … Cano, M. (2010). Analysis of subsidence using TerraSAR-X data: Murcia case study. *Engineering Geology*, *116*(3–4), 284–295.

Katagas, C., Tsolis-Katagas, P., & Baltatzis, E. (1991). Chemical mineralogy and illite crystallinity in low grade metasediments, Zarouchla Group, Northern Peloponnesus, Greece. *Mineralogy and Petrology*, *44*(1–2), 57–71.

Klose, M., Damm, B., & Terhorst, B. (2015). Landslide cost modeling for transportation infrastructures: A methodological approach. *Landslides*, *12*(2), 321–334. journal article. Retrieved from http://dx.doi.org/10.1007/s10346-014-0481-1

Koukis, G., Sabatakakis, N., Ferentinou, M., Lainas, S., Alexiadou, X., & Panagopoulos, A. (2009). Landslide phenomena related to major fault tectonics: Rift zone of Corinth Gulf, Greece. *Bulletin of Engineering Geology and the Environment*, *68*(2), 215–229.

Nichol, J., & Wong, M. (2005). Detection and interpretation of landslides using satellite images. *Land Degradation & Development*, *16*(3), 243–255.

Nikas, K., Antonakos, A., Lambrakis, N., & Kallergis, G. (2007). The use of antecedent precipitation index and delay factor to estimate runoff from rainfall: A case study from eight drainage basins-Achaia, Peloponessos, Greece. *Bulletin of the Geological Society of Greece*, *37*, 523–535.

Novellino, A., Cigna, F., Brahmi, M., Sowter, A., Bateson, L., & Marsh, S. (2017). Assessing the Feasibility of a National InSAR Ground Deformation Map of Great Britain with Sentinel-1. *Geosciences*, *7*(2), p 19. Retrieved from http://www.mdpi.com/2076-3263/7/2/19 doi;

Ori, G.G. (1989). Geologic history of the extensional basin of the Gulf of Corinth (? Miocene-Pleistocene), Greece. *Geology*, *17*(10), 918–921.

Piper, D.J. (2006). Sedimentology and tectonic setting of the Pindos Flysch of the Peloponnese, Greece. *Geological Society, London, Special Publications*, *260*(1), 493–505.

Psychogyiou, C., Papoutsis, I., Kontoes, C., Poyiadji, E., Spanou, N., & Klimis, N. (2015). Multi-temporal monitoring of slow moving landslide in South Pindus mountain range, Greece. *FRINGE 2015, (Vol. 731)*.

Raspini, F., Loupasakis, C., Rozos, D., Adam, N., & Moretti, S. (2014). Ground subsidence phenomena in the Delta municipality region (Northern Greece): Geotechnical modeling and validation with Persistent Scatterer Interferometry. *International Journal of Applied Earth Observation and Geoinformation*, *28*, 78–89.

Raspini, F., Loupasakis, C., Rozos, D., & Moretti, S. (2013). Advanced interpretation of land subsidence by validating multi-interferometric SAR data: The case study of the Anthemountas basin (Northern Greece). *Natural Hazards and Earth System Science*, *13*(10), 2425–2440.

Righini, G., Pancioli, V., & Casagli, N. (2012). Updating landslide inventory maps using Persistent Scatterer Interferometry (PSI). *International Journal of Remote Sensing*, *33*(7), 2068–2096.

Sanabria, M., Guardiola-Albert, C., Tomás Jover, R., Herrera García, G., Prieto, Á., Sánchez, H., & Tessitore, S. (2014). *Subsidence activity maps derived from DInSAR data: Orihuela case study*. Natural Hazards and Earth System Sciences Discussions, 1, 5365-5402.

Schuster, R.L., & Highland, L. (2001). *Socioeconomic and environmental impacts of landslides in the western hemisphere*. US Department of the Interior, US Geological Survey.

Shepard, D. (1968). *A two-dimensional interpolation function for irregularly-spaced data*. Proceedings of the 1968 23rd ACM national conference.

Solari, L., Raspini, F., Del Soldato, M., Bianchini, S., Ciampalini, A., Ferrigno, F., … Casagli, N. (2018). Satellite radar data for back-analyzing a landslide event: The Ponzano (Central Italy) case study. *Landslides*, *15*, 773–782.

Strozzi, T., Ambrosi, C., & Raetzo, H. (2013). Interpretation of aerial photographs and satellite SAR interferometry for the inventory of landslides. *Remote Sensing*, *5*(5), 2554–2570.

Tofani, V., Del Ventisette, C., Moretti, S., & Casagli, N. (2014). Integration of remote sensing techniques for intensity zonation within a landslide area: A case study in the northern Apennines, Italy. *Remote Sensing*, *6*(2), 907–924.

Van Westen, C.J. (2000). The modelling of landslide hazards using GIS. *Surveys in Geophysics*, *21*(2–3), 241–255.